## **RESEARCH PAPER**

# Carbon Quantum Dot Doping for Enhanced Power Conversion Efficiency in CsEuCl, Perovskite Solar Cells

Hayder Hasan Ali 1,2\*, Majid R. Al-bahrani 1

- <sup>1</sup> Department of Physics, College of Science, University of Thi-Qar, Thi-Qar, Iraq
- <sup>2</sup> Department of Science, College of Basic Education, University of Sumer, Thi-Qar, Iraq

#### ARTICLE INFO

#### Article History:

Received 05 September 2025 Accepted 29 November 2025 Published 01 January 2026

#### Keywords:

Halide perovskite Lead-free Rare earth Solar Cells

#### **ABSTRACT**

This study investigates the enhancement of power conversion efficiency (PCE) in lead-free CsEuCl<sub>2</sub> perovskite solar cells (PSCs) synthesized via the hot-injection method, which ensures precise crystallinity and phase purity. The perovskite layer was doped with carbon quantum dots (CQDs, 1-5 wt%), and the fabricated devices underwent comprehensive morphological (FESEM, XRD, and TEM), optical (UV-Vis), and electrical (J-V) characterizations to evaluate their performance. Optical analysis revealed bandgap reduction (from 1.74 eV to 1.52 eV at 3% CQDs) and enhanced absorption due to improved charge transport and suppressed recombination. Electrical performance peaked at 3% CQDs, achieving a PCE of 1.10% (vs. 0.78% for undoped cells), driven by optimized Jsc (10.5 mA/cm<sup>2</sup>) and retained Voc (0.34 V). Excessive doping (5% CQDs) induced CQD aggregation, degrading film morphology and performance. These findings underscore CQDs as a promising modifier for tuning optoelectronic properties in rare-earth-based PSCs, while the integrated characterization approach validates the structure-property relationships across all cell components.

## How to cite this article

Hasan Ali H., Al-bahrani M. Carbon Quantum Dot Doping for Enhanced Power Conversion Efficiency in CsEuCl<sub>3</sub> Perovskite Solar Cells. J Nanostruct, 2026; 16(1):375-386. DOI: 10.22052/JNS.2026.01.033

#### **INTRODUCTION**

Solar energy is a primary source of renewable and clean energy due to its quantity, purity, inexhaustibility, and its use does not harm the environment [1]. In the past few years, many methods have been developed to harness solar energy, such as artificial photosynthesis [2], solar architecture [3], solar thermal heaters [4] and photovoltaics (PV) [5]. Photovoltaic (PV) solar energy represents a key solution for reducing carbon emissions and meeting future energy demands [6]. This technology operates through the photoelectric effect, where sunlight is directly

converted into electricity using solar cells [7].

Recently, perovskite solar cells (PSCs) have emerged as a promising alternative to siliconbased PV, achieving over 25% efficiency with potential for further improvement [8[9]. The field began in 2009 when researchers used methylammonium lead bromide (MAPbBr3) as a photosensitizer in dye-sensitized cells, reaching 3.8% efficiency and sparking widespread interest in perovskite photovoltaics [10,11].

Perovskites are materials with  $ABX_3$  crystal structure, where "A" represents organic and inorganic cations, such as cesium (Cs $^+$ ),

<sup>\*</sup> Corresponding Author Email: hdoun1992@gmail.com

methylammonium (MA<sup>+</sup>, CH<sub>3</sub>NH<sub>3</sub><sup>+</sup>), and formamidine (FA<sup>+</sup>, CH<sub>3</sub>CH<sub>2</sub>NH<sub>3</sub><sup>+</sup>). "B" represents metal cations, such as tin cation (Sn<sup>2+</sup>), lead cation (Pb<sup>2+</sup>), etc. "X" represents halide groups, such as bromide (Br), iodide (I), and chloride (Cl). Perovskites have tunable band gaps (1.3-2.2 eV) [12], a high absorption coefficient (5.7 × 104 cm<sup>-1</sup> at 600 nm) [13,14], and effective charge carrier mobility (1-10 cm<sup>2</sup> V<sup>-1</sup> s<sup>-1</sup>) [15].

Organic-inorganic hybrid perovskites (OHIPs) now dominate solar cell research due to their low-cost fabrication and record efficiencies, building upon their 1990s applications in LEDs/transistors [16][17]. These materials exhibit superior optoelectronic characteristics including low exciton binding energy, large Bohr radius, high dielectric constant, extended carrier diffusion lengths, rapid charge mobility, and outstanding absorption coefficients [18,19].

The ABX<sub>3</sub> perovskite active layer absorbs photons, generating excitons that dissociate into free electrons (e<sup>-</sup>) and holes (h<sup>+</sup>). These charges are selectively extracted by the adjacent ETL (n-type) and HTL (p-type), respectively. Electrons flow through the ETL to the cathode via the external circuit, while holes migrate through the HTL to the anode, completing the electrical circuit. Simultaneously, the oxidized perovskite layer is regenerated through hole injection from the HTL, maintaining continuous operation [20].

Commonly used ETL materials in PSCs include

ZnO [21-23], TiO<sub>2</sub> [24-26], SnO<sub>2</sub> [27], WS<sub>2</sub> [28], TiS<sub>2</sub> [29], and MoS<sub>2</sub> [30]. The HTL significantly enhances PSC efficiency through optimized hole transport from perovskite to anode, with material doping strategies improving conductivity and reducing interfacial recombination [31]. However, lead toxicity in perovskites raises serious health concerns, including neurological, reproductive and renal damage [32]. driving research into lead-free alternatives [33].

Therefore, to make photovoltaics affordable and environmentally friendly, it is necessary to develop lead-free or lead-reduced perovskites [34,35]. The search for lead-free perovskite nanocrystals with low or no toxicity, good photovoltaic performance, and high environmental stability is in full swing. Due to the rich structure and elements of the perovskite family, many lead-free perovskite halide nanocrystals have been developed and characterized in the past few years. So far, Sn(II) [36], Sn(IV) [37], Sb(III) [38], Bi(III) [39], Cu(I) [40], Ag(I) [41], Na(I) [42], Yb(II) [43], and Eu(II) [44] have been used to replace lead. Some of these crystals exhibit decent optoelectronic performance comparable to their lead-based counterparts. These encouraging results in the exploration of lead-free perovskite nanocrystals show promising signs for the breakthrough in the fabrication of novel optoelectronic devices.

Europium (Eu) serves as an effective lightsensing element in perovskites [45]. Eu<sup>2+</sup>

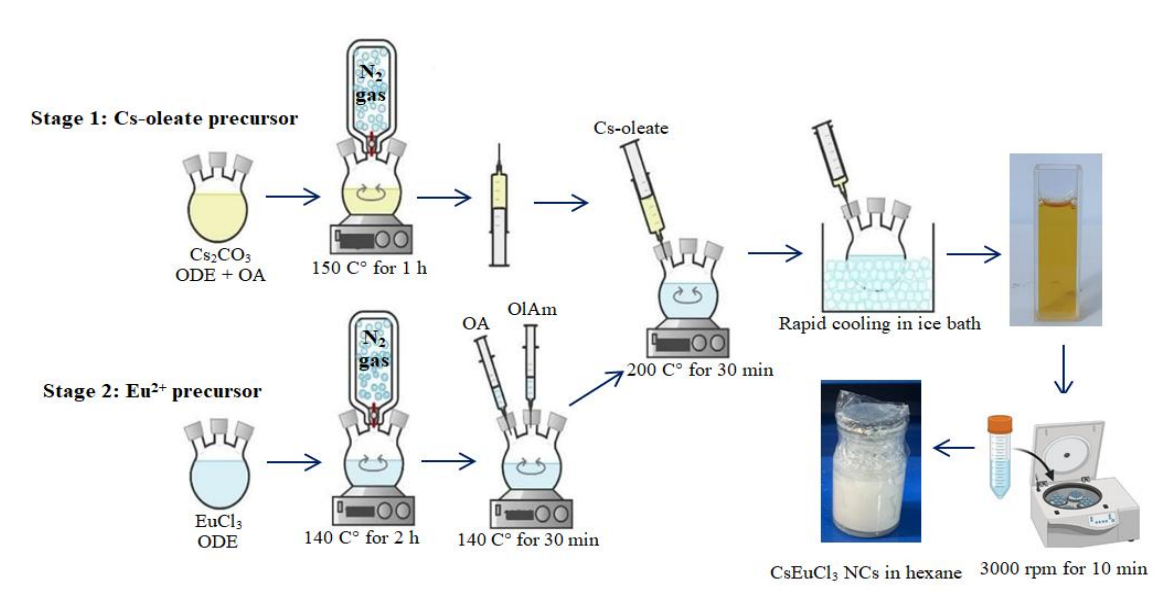


Fig. 1. Schematic diagram of CsEuCl<sub>3</sub> nanocrystals synthesis and purification via hot-injection method.

incorporation enhances structural stability due to its similar ionic radius to Pb<sup>2+</sup> (117 pm vs. 119 pm) and favorable octahedral coordination [46,47]. While solid-state synthesis of bulk Eu-halide perovskites faces homogeneity and shape control limitations, colloidal methods enable improved uniformity and morphology tuning. Recent studies focus on CsBr:Eu<sup>2+</sup> nanocrystals, though pure Eu-halide perovskites remain synthetically challenging [47,48].

This study presents a systematic investigation of hot-injection-grown perovskite CsEuCl3 nanocrystals for solar cell applications using titanium dioxide/nickel dioxide charge-transport layers. Four different device structures were studied: a pure reference cell and cells containing different percentages of carbon quantum dots, to comprehensively evaluate their optical and photovoltaic effects.

#### **MATERIALS AND METHODS**

Synthesis and Purification of CsEuCl, Nanocrystals

The Cs-oleate precursor was prepared by reacting  $Cs_2CO_3$  (0.25 g) with oleic acid (0.5 mL) in octadecene (8 mL) at 150°C under  $N_2$  atmosphere. For nanocrystal synthesis, EuCl<sub>3</sub> (0.27 g) was dissolved in octadecene (5 mL) at 140°C under vacuum, followed by  $N_2$  purging and injection of oleylamine/oleic acid (0.5 mL each). After 30 min, the temperature was raised to 200°C for rapid injection of preheated Cs-oleate (0.4 mL). The reaction was quenched after 1 min in an ice bath, then purified via two-step centrifugation (3000 rpm, 10 min) with hexane washing. The final CsEuCl<sub>3</sub> nanocrystals were stored in hexane at 4°C

for characterization.

Synthesis of CsEuCl<sub>3</sub>:CQDs Nanocomposites

The nanocomposites were prepared through a facile and cost-effective solution-phase method employing commercially available solvents. In a typical synthesis, 4 mL of CsEuCl<sub>3</sub> nanocrystal solution was introduced into a 25 mL three-neck flask under continuous N<sub>2</sub> purge at 120 °C. Subsequently, carbon quantum dots (CQDs) were incorporated at varying mass ratios (1, 3, and 5 wt%), with rigorous stirring maintained for 60 minutes to ensure homogeneous dispersion and effective composite formation. The resulting CsEuCl<sub>3</sub>:CQD nanocomposite solutions were subsequently stored at 4°C in sealed vials to prevent degradation prior to characterization.

## Preparation and Deposition of TiO, as ETLs

A stable TiO $_2$  paste was prepared by dispersing anatase nanoparticles (20–30 nm) in an acidic aqueous solution (acetic acid/DI water), followed by adding ethanol and  $\alpha$ -terpineol under continuous stirring. The paste was spin-coated onto masked FTO substrates (1000 rpm/10 s  $\Rightarrow$  3000 rpm/30 s) to form ~150 nm films, which were soft-baked at 115°C and then sintered with a graded thermal treatment (100–450°C) to produce crack-free, crystalline electron transport layers for efficient perovskite solar cells. See Fig. 2.

Deposition of CsEuCl<sub>3</sub> and CsEuCl<sub>3</sub>:CQD onto ETLs Thin Films

The CsEuCl<sub>3</sub> perovskite nanocrystals (NCs) were deposited via spin-coating (2000 rpm, 30 sec) onto

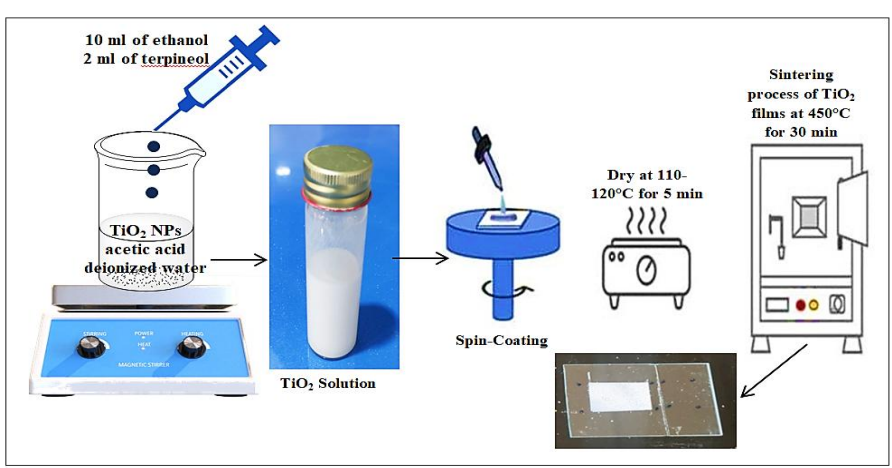


Fig. 2. Preparation and deposition of  ${\rm TiO_2}$  thin films onto the FTO glass as ETLs.

both TiO<sub>2</sub> thin films, followed by thermal annealing at 100-120°C for 5-10 min under a nitrogen atmosphere to enhance film quality. Subsequently, CsEuCl<sub>3</sub>:CQD nanocomposites with varying CQD concentrations (1, 3, and 5 wt%), resulting in four distinct thin film architectures: TiO<sub>2</sub>/CsEuCl<sub>3</sub>, TiO<sub>2</sub>/CsEuCl<sub>3</sub>:CQDs (1 wt%), TiO<sub>2</sub>/CsEuCl<sub>3</sub>:CQDs (3 wt%), and TiO<sub>2</sub>/CsEuCl<sub>3</sub>:CQDs (5 wt%). This systematic approach enabled a comparative investigation of the effects of graphene incorporation and CQD doping concentration on the structural and optoelectronic properties of the perovskite NC films.

#### Deposition of NiO as a HTL on Thin Films

The NiO HTL was prepared by dissolving 1.44 g NiO nanoparticles in 4 mL HCl at 75°C for 15 min [49][50]. This solution was spin-coated uniformly onto all fuor device configurations. All samples were annealed at 100°C for 10 min in air to ensure optimal adhesion and crystallinity, completing the device architecture while enabling direct comparison of charge transport properties across different perovskite compositions. See Fig. 3.

Finally, a Cu NPs counter electrode was thermally evaporated (<5×10<sup>-6</sup> Torr) on all four device stacks. Current density-voltage (J-V) characteristics were measured under AM1.5G illumination (100 mW/cm²) using a Keithley 4250 system (Sciencetech solar simulator).

#### **RESULTS AND DISCUSSION**

Structural characterization

Fig. 4a shows pure CsEuCl<sub>3</sub> crystals with a dense, uniform grain structure. Introducing 1% CQDs (Fig. 4b) induces slight structural modifications,

suggesting potential improvements in optical properties such as absorbance and bandgap tuning. A more pronounced enhancement is observed in Fig. 4c (3% CQDs), where the perovskite exhibits a highly ordered morphology with reduced intergranular spacing. This optimized structure enhances light absorption and charge transport, making it ideal for perovskite solar cells. However, at 5% CQDs (Fig. 4d), excessive nanoparticle loading leads to large, irregular aggregates that likely hinder charge transport and introduce defects. These results highlight 3% CQDs as the optimal concentration, balancing structural integrity and optoelectronic performance for solar cell applications.

Fig. 5a depicts the TiO<sub>2</sub> electron-transport layer, exhibiting a nanoporous structure with well-interconnected grains. This morphology is essential for minimizing electrical resistance and promoting efficient electron transport, thereby reducing charge recombination and enhancing device stability. Fig. 5b illustrates the NiO hole-transport layer, characterized by densely packed nanoclusters with a homogeneous distribution. This compact structure ensures efficient hole transport while minimizing voltage losses, thereby improving interfacial compatibility with the perovskite layer and overall device performance.

Collectively, these microstructural analyses confirm that all three layers possess optimal morphological properties for high-performance perovskite solar cells. The CsEuCl<sub>3</sub> absorber enables effective light harvesting, the TiO<sub>2</sub> layer facilitates unhindered electron transport, and the NiO layer ensures efficient hole extraction collectively contributing to enhanced device

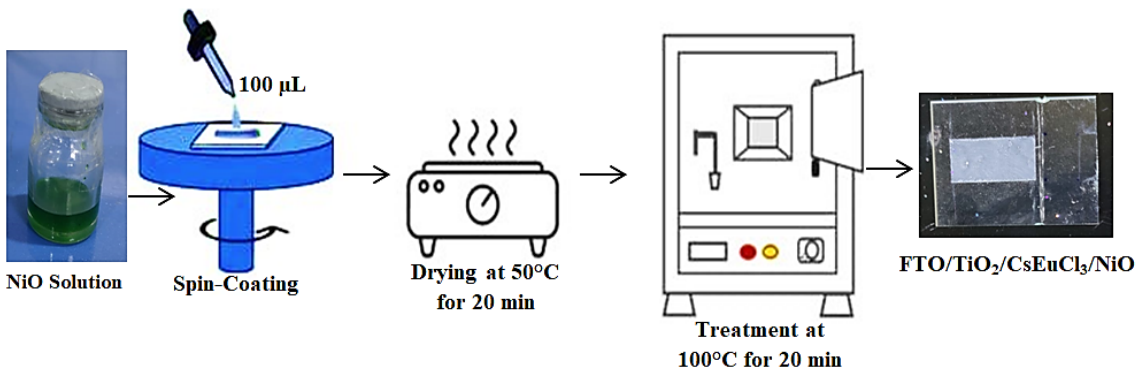


Fig. 3. Shows NiO deposited by spin-coating on a Thin Films substrate.

efficiency and long-term stability.

XRD analysis of TiO<sub>2</sub> NPs (Fig. 6a) confirms an anatase phase with dominant (011) and (004) planes at 25.034° and 37.579°, showing crystallite

sizes of 6.3-18.3 nm. While the anatase structure favors electron transport, size variations may introduce minor defects. For NiO NPs (Fig. 6b), sharp peaks matching cubic phase (JCPDS 96-

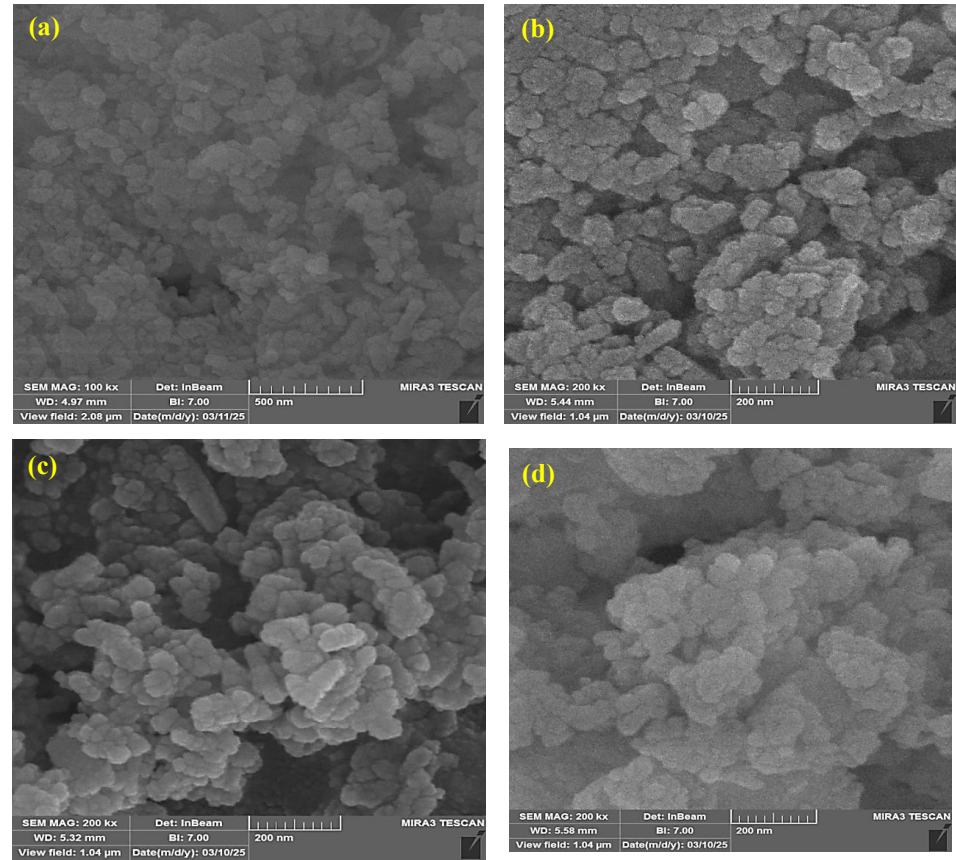


Fig. 4. FE-EM characterization of the perovskite nanocrystal structures: (a) Pure CsEuCl<sub>3</sub>, (b) with 1wt% CQDs, (c) with 3wt% CQDs, and (d) with 5wt% CQDs.

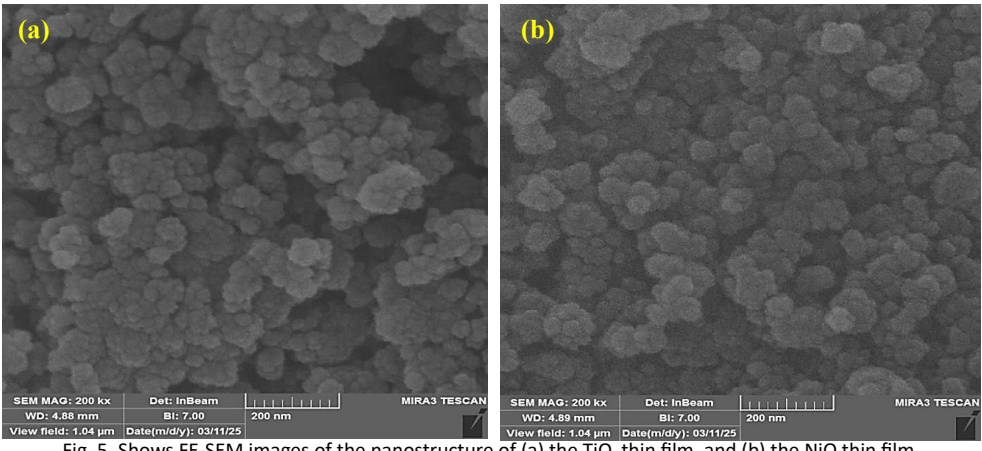


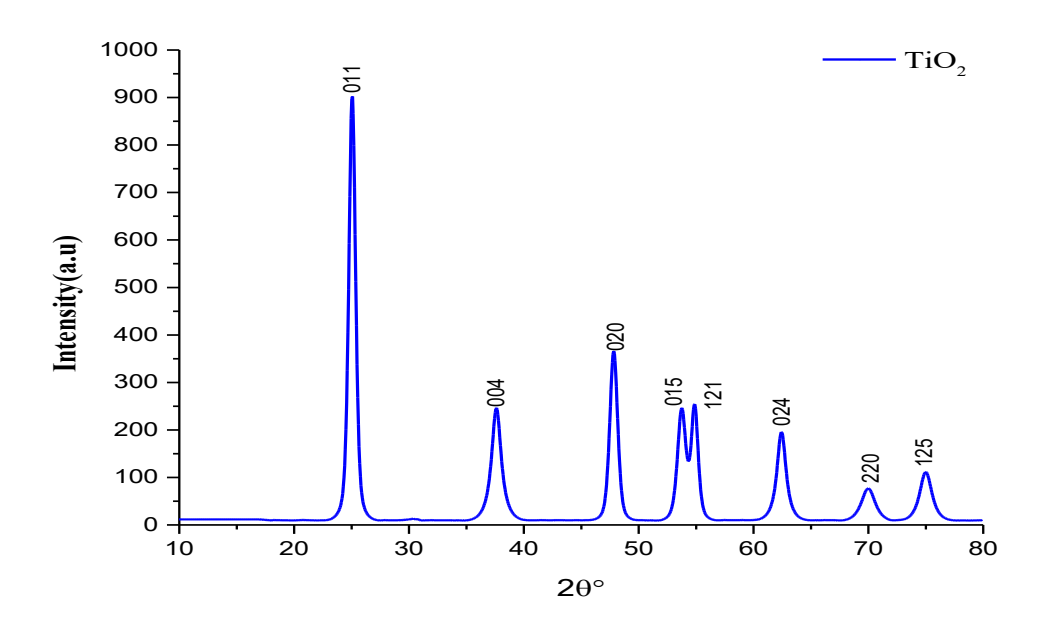
Fig. 5. Shows FE-SEM images of the nanostructure of (a) the TiO<sub>2</sub> thin film, and (b) the NiO thin film.

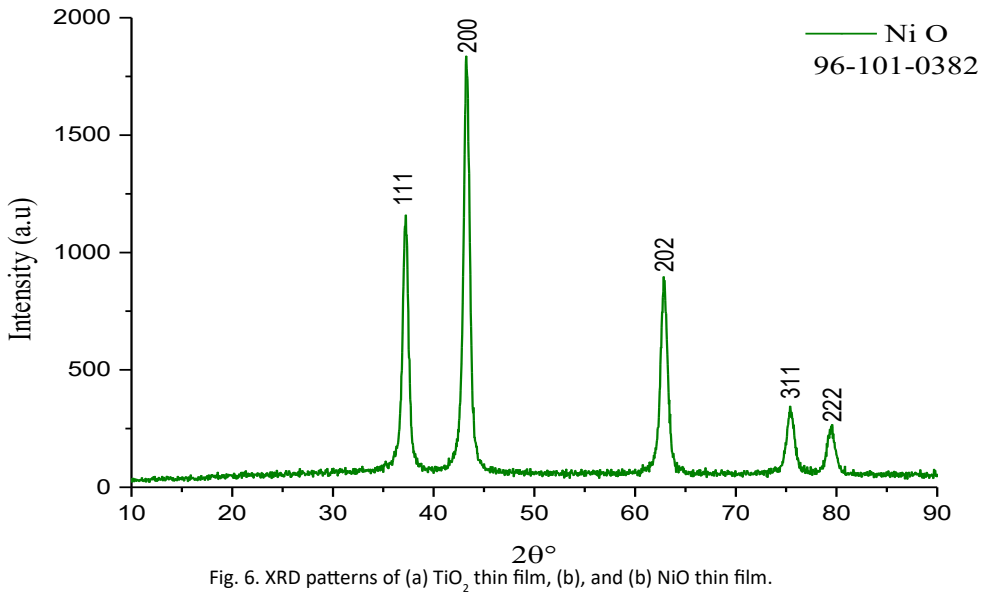
101-0382) with 10.86 nm average crystallite size and narrow FWHM (0.74-0.97°) demonstrate high crystallinity and phase purity. Both materials exhibit suitable structural properties for their respective roles as electron (TiO<sub>2</sub>) and hole (NiO) transport layers in perovskite solar cells, as further supported by FE-SEM observations (Fig. 5).

To investigate whether the addition of CQDs would alter the crystal structure of CsEuCl<sub>2</sub>, the XRD patterns of pure CsEuCl<sub>3</sub> film and CsEuCl<sub>3</sub> films

with different proportions of CQDs are shown in Fig. 7. The XRD results were found to be in good agreement with the standard pattern of CsEuCl<sub>3</sub> NCs. The lattice constants of the (111), (112), (101), (211), and (222) crystal planes were determined to be 26.57, 32.74, 37.63, 51.11, and 54.83 Å, respectively, based on the tetragonal phase.

When CQDs were added to CsEuCl, perovskite crystals at concentrations of 1 and 3%, and X-ray diffraction (XRD) analysis was performed, no





new peaks appeared. This is attributed to the insufficient concentration of CQDs to exceed the critical threshold required for structural modification. However, the appearance of the (100) diffraction peak at angle 41.88° in the 5% CQDs sample, but not in its lower concentration counterparts, reflects the occurrence of a critical structural change at this ratio, where the quantum dot concentration exceeds the structural effect threshold (~4.2%) to form an interconnected network, causing sufficient lattice strain to distort the Eu-Cl bond angles, leading to a decrease in absorbance and an increase in the optical energy

Transmission electron microscopy (TEM) images from this study demonstrate a clear evolution in the nanostructure of CsEuCl3 perovskite crystals upon the addition of carbon quantum dots (CQDs). Fig. 8a shows CsEuCl3 perovskite crystals with cubic and rectangular morphologies exhibiting

distinct size distribution variations. The cubic morphology reflects the optimal crystal structure of the ABX3 system with cubic symmetry, indicating sample purity and the absence of major defects, consistent with previous studies reporting such crystal structures in metal halide nanostructures.

With the incorporation of 1% CQDs (Fig. 8b), small nanoparticles (<10 nm) appear distributed sparsely on the perovskite surface while maintaining the compound's basic structure, potentially leading to modest optical property enhancements. Fig. 8c (3% CQDs) demonstrates optimal quantum dot distribution, where homogeneous dispersion within the perovskite matrix forms effective crystal interfaces, resulting in improved absorbance and reduced energy gap (Eg). In contrast, Fig. 8d (5% CQDs) reveals significant quantum dot clustering, causing perovskite crystal structure distortions and increased defect density. These morphological changes impede charge transport, reduce electron-

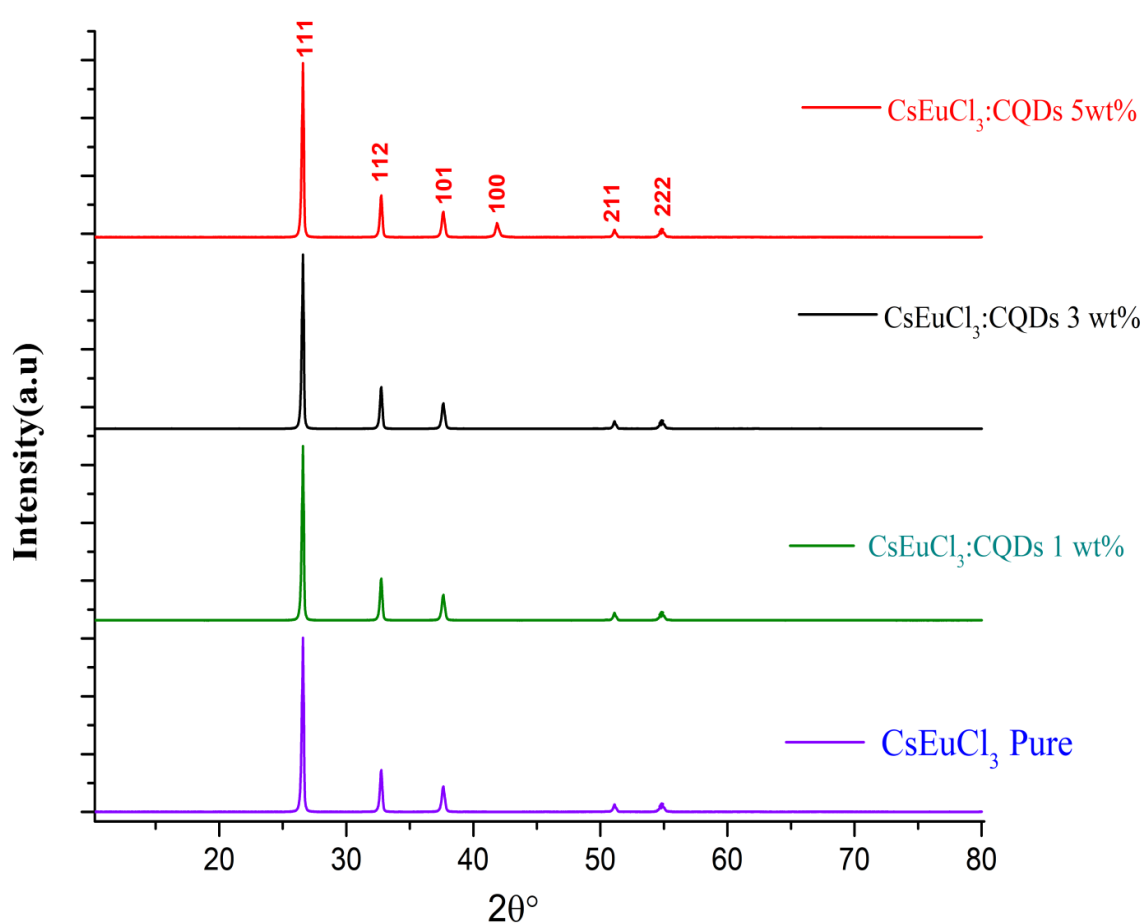


Fig. 7. XRD patterns of pure CsEuCl<sub>3</sub> film and CsEuCl<sub>3</sub> films with different concentrations of CQDs additives.

hole separation efficiency, and initiate gradual property degradation. The results establish that 3% CQDs incorporation represents the optimal concentration, achieving both homogeneous quantum dot distribution and preservation of CsEuCl3 optical and electrical properties.

## Optical characterization

The incorporation of carbon quantum dots (CQDs) into lead-free CsEuCl3 perovskite nanocrystals results in significant modifications to their optical absorption properties and bandgap energies, as demonstrated by UV-Vis spectroscopy (Fig. 9) and Tauc plot analysis (Fig. 10). A significant improvement in absorption was observed in the wavelength range of 400–850 nm compared to the pure thin film. This enhancement can be attributed

to the role of CQDs as charge transport mediators within the perovskite structure, suppressing non-radiative recombination and increasing the effective surface area of the CsEuCl3 NCs. These effects collectively improve the efficiency of light absorption and electron-hole pair generation. However, a decrease in absorbance was observed for the thin film with 5wt% CQDs. This reduction may be due to the clustering of quantum dots at higher concentrations, leading to non-uniform dispersion, hindered charge transport, and the introduction of defects in the perovskite structure (as confirmed by TEM). Additionally, the clustered CQDs may act as light-blocking agents, preventing photons from reaching the CsEuCl3 NCs and thereby reducing absorption [51].

Fig. 10 shows the bandgap design of perovskite

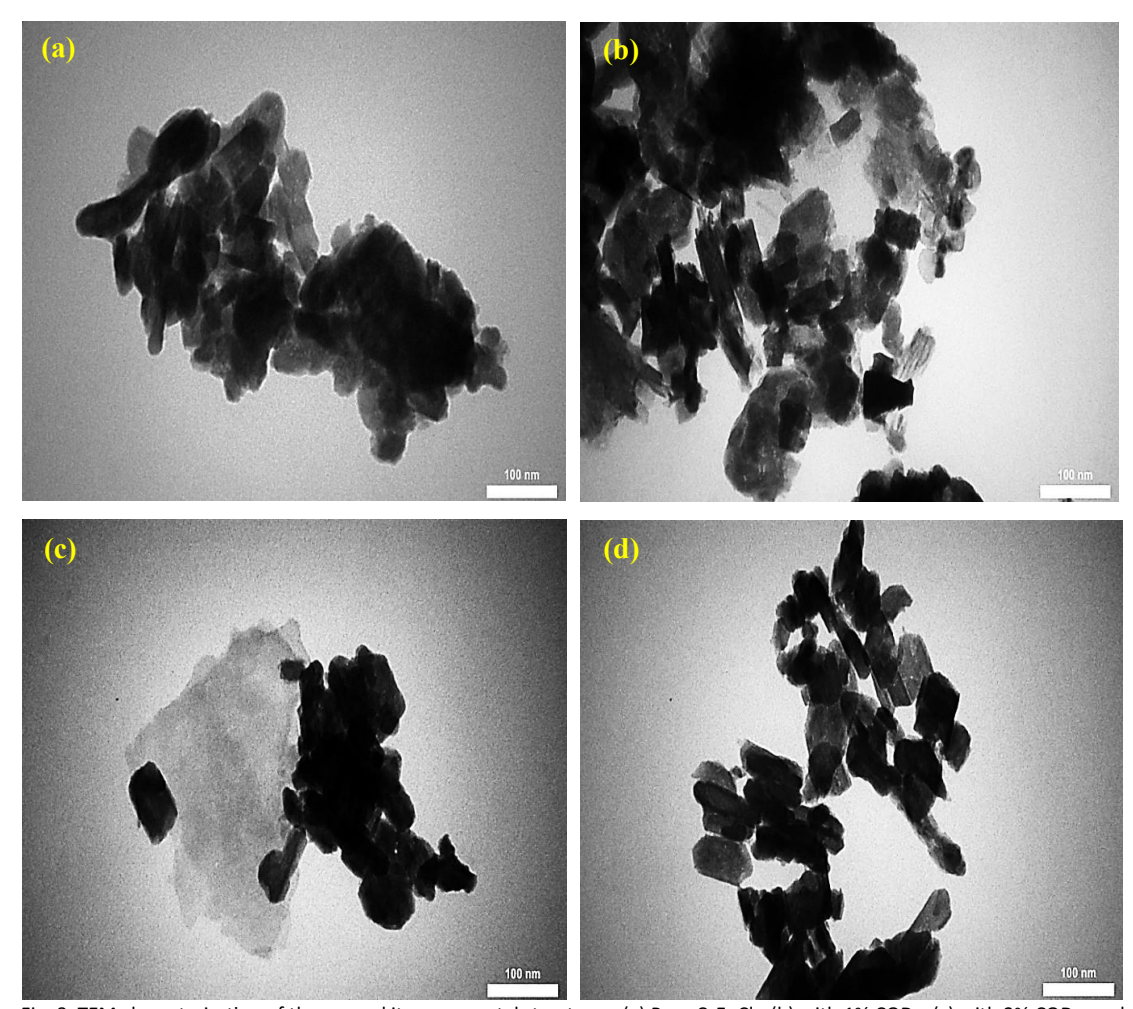


Fig. 8. TEM characterization of the perovskite nanocrystal structures: (a) Pure CsEuCl<sub>3</sub>, (b) with 1% CQDs, (c) with 3% CQDs, and (d) with 5% CQDs.

solar cells using colloidal quantum dots (CQDs) incorporation, demonstrating an ideal doping range of 1% to 3%. This reduces the bandgap

from 1.67 eV to 1.52 eV through intermediate state formation and band edge modification, enhancing solar spectrum matching and charge

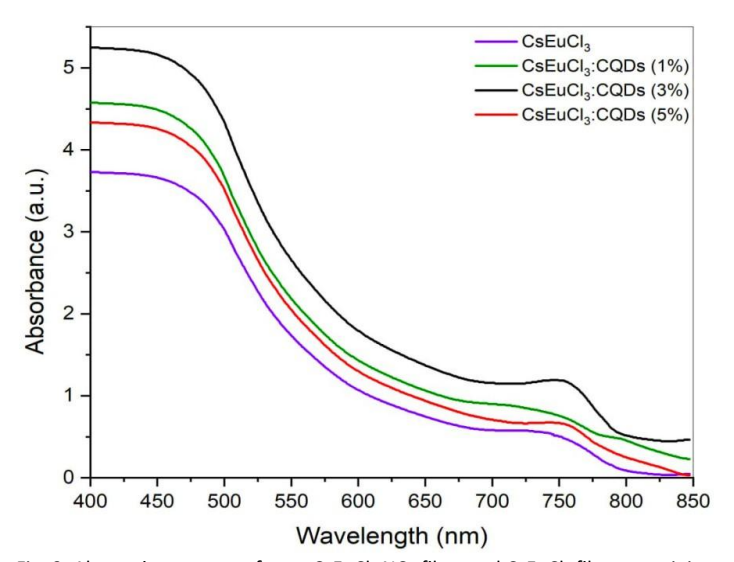
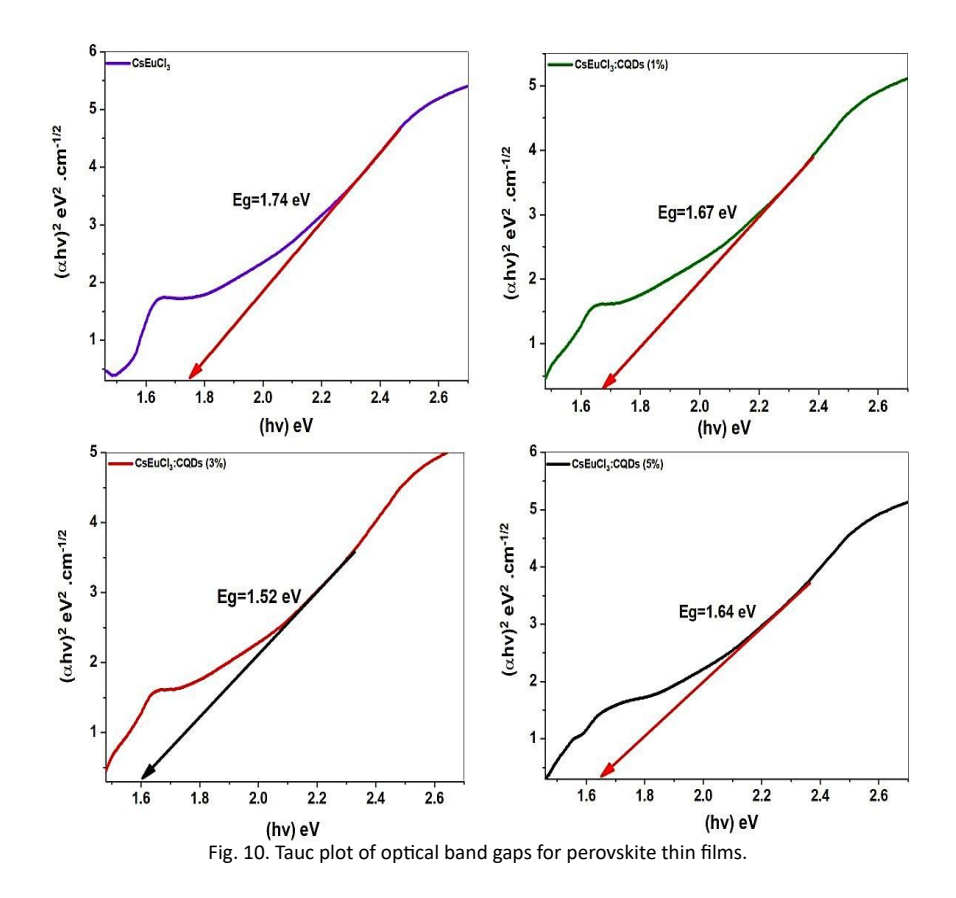


Fig. 9. Absorption spectra of pure  ${\sf CSEUCl_3}$  NCs films and  ${\sf CSEUCl_3}$  films containing different proportions of CQDs.



transport. However, a CQD loading of 5% induces nanoparticle aggregation and lattice stress, which increases the bandgap and impairs photovoltaic performance, demonstrating a clear concentration threshold for achieving optimal device efficiency.

## Electrical characterization

The photovoltaic parameters of the four perovskite solar cells (H1-H4) with distinct architectures: (H1=FTO/TiO2/CsEuCl3/NiO/Cu), (H2=FTO/TiO2/CsEuCl3:CQDs 1%/NiO/

Cu), (H3=FTO/TiO2/CsEuCl3:CQDs 3%/NiO/Cu), (H4=FTO/TiO2/CsEuCl3:CQDs 5%/NiO/Cu)), summarized in Table 1, reveal a clear correlation between device composition, optical bandgap tuning via carbon quantum dots (CQDs), and electrical performance. The reference cell H1 (CsEuCl3, Eg = 1.74 eV) exhibits the lowest PCE (0.78%) due to its wide bandgap, limiting light absorption, and poor charge transport (FF = 0.327). Incorporation of 1% CQDs in H2 (Eg = 1.67 eV) slightly enhances Jsc (7.9 mA/cm²) but

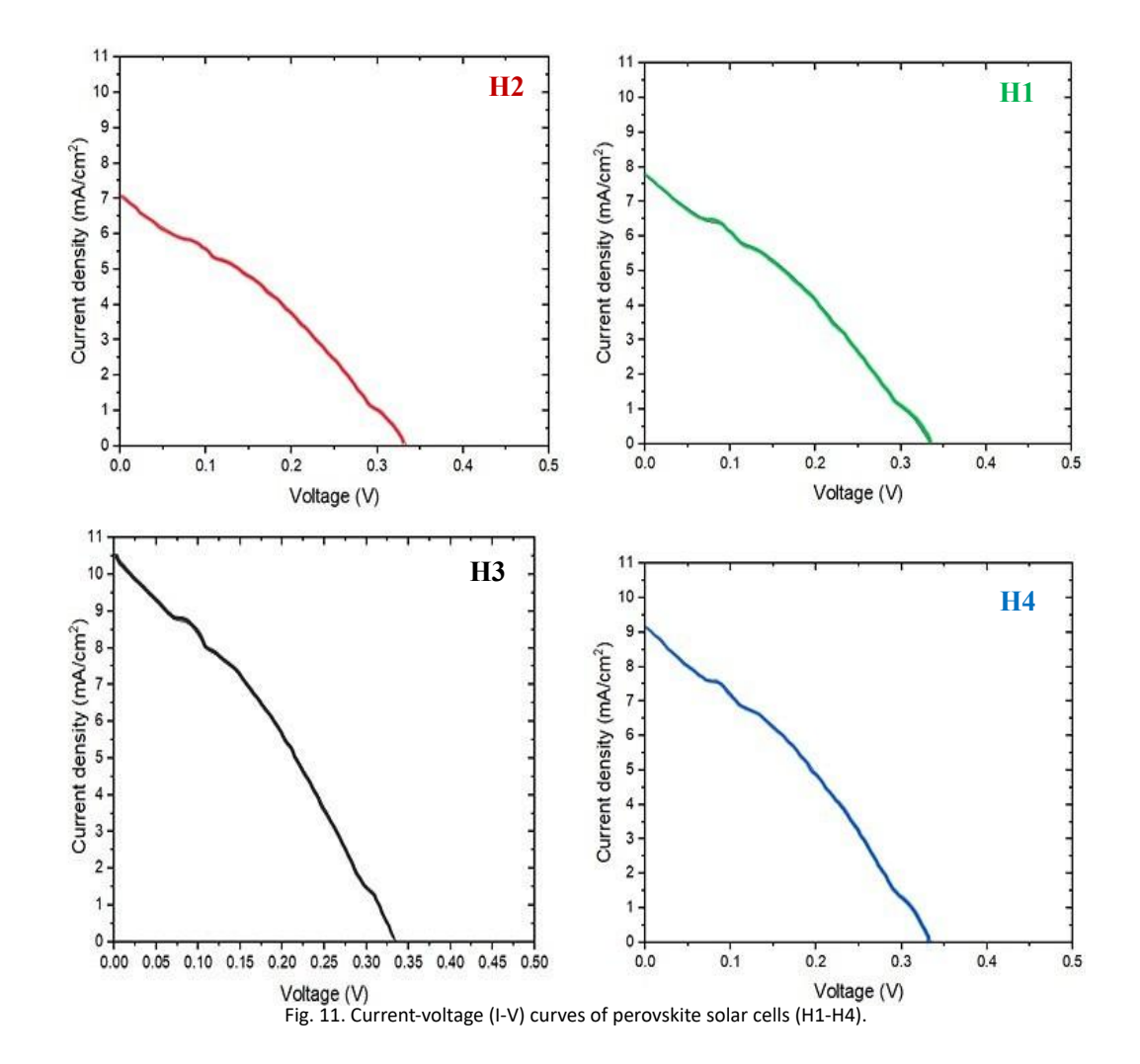


Table 1. Electrical characteristics of perovskite solar cells (H1-H4)

Table 1. Electrical characteristics of perovskite solar cens (111-114)				
Device	H1	H2	Н3	H4
Jsc mA.cm <sup>-2</sup>	7	7.9	10.5	9.1
Voc V	0.34	0.34	0.34	0.33
FF	0.327	0.312	0.308	0.333
PCE %	0.78	0.84	1.10	1.00

reduces FF (0.312), likely due to interfacial defects or incomplete passivation. Notably, H3 (3% CQDs, Eg = 1.52 eV) achieves the highest PCE (1.10%) owing to its optimal bandgap for visible-light harvesting, reflected in the improved Jsc (10.5 mA/cm²), though FF remains low (0.308), suggesting persistent recombination losses. Conversely, H4 (5% CQDs, Eg = 1.60 eV) shows intermediate performance (PCE = 1.00%), indicating that excessive CQD doping may introduce trap states or phase impurities, as evidenced by its reduced Voc (0.33 V) compared to H1-H3 (0.34 V).

The IV curves (Fig. 11) further highlight these trends: H3 demonstrates the highest current density, while H1 and H2 exhibit significant series resistance (slope near Voc). The data underscore that CQD incorporation—particularly at 3%—effectively narrows the bandgap and enhances charge generation, but further interfacial engineering is required to mitigate recombination and boost FF.

#### **CONCLUSION**

The integration of CQDs into CsEuCl, perovskite nanocrystals demonstrated a profound impact on both optical and electrical characteristics. At 3% CQD loading, the bandgap narrowed to 1.52 eV, enhancing visible-light absorption and charge generation, while TEM and XRD confirmed preserved crystallinity and homogeneous dispersion. This optimization translated to a 41% increase in PCE (1.10%) compared to undoped devices, driven by higher J2c and minimal Voc loss. However, exceeding the optimal doping concentration (5% CQDs) led to quantum dot clustering, lattice strain, and increased defect density, reversing performance gains. The study underscores the delicate balance between CQDinduced bandgap engineering and morphological stability.

## **CONFLICT OF INTEREST**

The authors declare that there is no conflict of interests regarding the publication of this manuscript.

## REFERENCES

- Celik I, Phillips AB, Song Z, Yan Y, Ellingson RJ, Heben MJ, et al. Environmental analysis of perovskites and other relevant solar cell technologies in a tandem configuration. Energy and Environmental Science. 2017;10(9):1874-1884.
- Zhen C, Chen X, Chen R, Fan F, Xu X, Kang Y, et al. Liquid metalembraced photoactive films for artificial photosynthesis. Nature Communications. 2024;15(1).

- Guo Y, Tsuda K, Hosseini S, Murakami Y, Tricoli A, Coventry J, et al. Scalable nano-architecture for stable nearblackbody solar absorption at high temperatures. Nature Communications. 2024:15(1).
- Ravi Kumar K, Krishna Chaitanya NVV, Sendhil Kumar N. Solar thermal energy technologies and its applications for process heating and power generation – A review. Journal of Cleaner Production. 2021;282:125296.
- Li Y, Huang X, Sheriff HKM, Forrest SR. Semitransparent organic photovoltaics for building-integrated photovoltaic applications. Nature Reviews Materials. 2022;8(3):186-201.
- Zhang H, Yu Z, Zhu C, Yang R, Yan B, Jiang G. Green or not? Environmental challenges from photovoltaic technology. Environ Pollut. 2023;320:121066.
- Dubey S, Sarvaiya JN, Seshadri B. Temperature Dependent Photovoltaic (PV) Efficiency and Its Effect on PV Production in the World – A Review. Energy Procedia. 2013;33:311-321.
- Cho KT, Paek S, Grancini G, Roldán-Carmona C, Gao P, Lee Y, et al. Highly efficient perovskite solar cells with a compositionally engineered perovskite/hole transporting material interface. Energy and Environmental Science. 2017;10(2):621-627.
- Noman M, Khan Z, Jan ST. A comprehensive review on the advancements and challenges in perovskite solar cell technology. RSC Advances. 2024;14(8):5085-5131.
- Kojima A, Teshima K, Shirai Y, Miyasaka T. Organometal Halide Perovskites as Visible-Light Sensitizers for Photovoltaic Cells. Journal of the American Chemical Society. 2009;131(17):6050-6051.
- Chen T, Liu R, Tang S, Li X, Ye S, Duan X, et al. Ni2+ doping induced structural phase transition and photoluminescence enhancement of CsPbBr<sub>3</sub>. AIP Advances. 2021;11(11).
- 12. Cheng J, Choi I, Kim W, Li H, Koo B, Ko MJ. Wide-Band-Gap (2.0 eV) Perovskite Solar Cells with a  $\rm V_{oc}$  of 1.325 V Fabricated by a Green-Solvent Strategy. ACS Applied Materials and Interfaces. 2023;15(19):23077-23084.
- Bhojak V, Jain PK, Bhatia D, Dargar SK, Jasinski M, Gono R, et al. Numerical Investigation of Power Conversion Efficiency of Sustainable Perovskite Solar Cells. Electronics. 2023;12(8):1762.
- 14. Chen Z, Li X, Guo X. Enhanced absorption in perovskite solar cells by incorporating gold triangle nanostructures. Appl Opt. 2023;62(19):5064.
- Dong Q, Fang Y, Shao Y, Mulligan P, Qiu J, Cao L, et al. Electronhole diffusion lengths and 175 μm in solution-grown CH<sub>3</sub>NH<sub>3</sub>Pbl<sub>3</sub> single crystals. Science. 2015;347(6225):967-970.
- Xiao Z, Meng W, Wang J, Mitzi DB, Yan Y. Searching for promising new perovskite-based photovoltaic absorbers: the importance of electronic dimensionality. Materials Horizons. 2017;4(2):206-216.
- Synergistic Effects of Lead Thiocyanate Additive and Solvent Annealing on the Performance of Wide-Bandgap Perovskite Solar Cells. American Chemical Society (ACS).
- Kim DH, Park J, Li Z, Yang M, Park JS, Park IJ, et al. 300% Enhancement of Carrier Mobility in Uniaxial-Oriented Perovskite Films Formed by Topotactic-Oriented Attachment. Adv Mater. 2017;29(23).
- Hoque MNF, Islam N, Li Z, Ren G, Zhu K, Fan Z. Ionic and Optical Properties of Methylammonium Lead Iodide Perovskite across the Tetragonal–Cubic Structural Phase Transition. ChemSusChem. 2016;9(18):2692-2698.
- 20. Gonzalez-Pedro V, Juarez-Perez EJ, Arsyad W-S, Barea EM,

- Fabregat-Santiago F, Mora-Sero I, et al. General Working Principles of CH<sub>3</sub>NH<sub>3</sub>PbX<sub>3</sub> Perovskite Solar Cells. Nano Lett. 2014;14(2):888-893.
- 21. Ali HH. Preparation and Characterization of ZnO NWs/ Graphene Nanocomposite as an Effective Photoanode Electrode for Improving the Performance of the Dye-Sensitized Solar Cells. University of Thi-Qar Journal of Science. 2023;10(1):11-15.
- Han GS, Shim HW, Lee S, Duff ML, Lee JK. Low-Temperature Modification of ZnO Nanoparticles Film for Electron-Transport Layers in Perovskite Solar Cells. ChemSusChem. 2017;10(11):2425-2430.
- Stable Electron-Transport-Layer-Free Perovskite Solar Cells with over 22% Power Conversion Efficiency. American Chemical Society (ACS). http://dx.doi.org/10.1021/acs. nanolett.2c04720.s001
- Prochowicz D, Tavakoli MM, Wolska-Pietkiewicz M, Jędrzejewska M, Trivedi S, Kumar M, et al. Suppressing recombination in perovskite solar cells via surface engineering of TiO<sub>2</sub> ETL. Solar Energy. 2020;197:50-57.
- Fabrication of a Highly Functional TiO<sub>2</sub>/AZO Bilayer Electron Transport Layer for Planar Perovskite Solar Cells. American Chemical Society (ACS).
- 26. Ramirez EB, Alonso JC, Huerta L. YSZ Thin Films Prepared by Spin Coating Method. ECS Meeting Abstracts. 2013;MA2013-01(26):1021-1021.
- 27. Jiang Q, Zhang X, You J. SnO<sub>2</sub>: A Wonderful Electron Transport Layer for Perovskite Solar Cells. Small. 2018;14(31).
- 28. Sobayel K, Akhtaruzzaman M, Rahman KS, Ferdaous MT, Al-Mutairi ZA, Alharbi HF, et al. A comprehensive defect study of tungsten disulfide (WS<sub>2</sub>) as electron transport layer in perovskite solar cells by numerical simulation. Results in Physics. 2019;12:1097-1103.
- 29. Yin G, Zhao H, Feng J, Sun J, Yan J, Liu Z, et al. Low-temperature and facile solution-processed two-dimensional TiS<sub>2</sub> as an effective electron transport layer for UV-stable planar perovskite solar cells. Journal of Materials Chemistry A. 2018;6(19):9132-9138.
- Singh R, Giri A, Pal M, Thiyagarajan K, Kwak J, Lee J-J, et al. Perovskite solar cells with an MoS<sub>2</sub> electron transport layer. Journal of Materials Chemistry A. 2019;7(12):7151-7158.
- 31. Chu Q-Q, Ding B, Peng J, Shen H, Li X, Liu Y, et al. Highly stable carbon-based perovskite solar cell with a record efficiency of over 18% via hole transport engineering. Journal of Materials Science and Technology. 2019;35(6):987-993.
- 32. Ju M-G, Chen M, Zhou Y, Dai J, Ma L, Padture NP, et al. Toward Eco-friendly and Stable Perovskite Materials for Photovoltaics. Joule. 2018;2(7):1231-1241.
- Chutia T, Kalita DJ. Rational design of mixed Sn–Ge based hybrid halide perovskites for optoelectronic applications: a first principles study. RSC Advances. 2022;12(39):25511-25519.
- 34. Wang X, Zhang T, Lou Y, Zhao Y. All-inorganic lead-free perovskites for optoelectronic applications. Materials Chemistry Frontiers. 2019;3(3):365-375.
- Fu H. Review of lead-free halide perovskites as lightabsorbers for photovoltaic applications: From materials to solar cells. Sol Energy Mater Sol Cells. 2019;193:107-132.
- 36. Lin R, Xiao K, Qin Z, Han Q, Zhang C, Wei M, et al. Monolithic all-perovskite tandem solar cells with 24.8% efficiency

- exploiting comproportionation to suppress Sn(ii) oxidation in precursor ink. Nature Energy. 2019;4(10):864-873.
- 37. Nakamura T, Yakumaru S, Truong MA, Kim K, Liu J, Hu S, et al. Sn(IV)-free tin perovskite films realized by in situ Sn(0) nanoparticle treatment of the precursor solution. Nature Communications. 2020;11(1).
- 38. Bright Blue and Green Luminescence of Sb(III) in Double Perovskite Cs2MInCl6 (M = Na, K) Matrices. American Chemical Society (ACS).
- Lyu M, Yun J-H, Cai M, Jiao Y, Bernhardt PV, Zhang M, et al. Organic–inorganic bismuth (III)-based material: A lead-free, air-stable and solution-processable light-absorber beyond organolead perovskites. Nano Research. 2016;9(3):692-702.
- Zhao X-G, Yang D, Sun Y, Li T, Zhang L, Yu L, et al. Cu–In Halide Perovskite Solar Absorbers. Journal of the American Chemical Society. 2017;139(19):6718-6725.
- 41. Yoon DY, Lim E, Kim YJ, Kim JH, Ryu T, Lee S, et al. NO oxidation activity of Ag-doped perovskite catalysts. J Catal. 2014;319:182-193.
- Retuerto M, Pascual L, Calle-Vallejo F, Ferrer P, Gianolio D, Pereira AG, et al. Na-doped ruthenium perovskite electrocatalysts with improved oxygen evolution activity and durability in acidic media. Nature Communications. 2019;10(1).
- Moon BJ, Kim SJ, Lee S, Lee A, Lee H, Lee DS, et al. Rare-Earth-Element-Ytterbium-Substituted Lead-Free Inorganic Perovskite Nanocrystals for Optoelectronic Applications. Adv Mater. 2019;31(33).
- 44. Kunkel N, Meijerink A, Springborg M, Kohlmann H. Eu(ii) luminescence in the perovskite host lattices KMgH<sub>3</sub>, NaMgH<sub>3</sub> and mixed crystals LiBaxSr<sub>1-x</sub>H<sub>3</sub>. J Mater Chem C. 2014;2(24):4799-4804.
- 45. ElectronPhonon Coupling in Luminescent Europium-Doped Hydride Perovskites Studied by Luminescence Spectroscopy, Inelastic Neutron Scattering, and First-Principles Calculations. American Chemical Society (ACS).
- 46. Swarnkar A, Mir WJ, Nag A. Can B-Site Doping or Alloying Improve Thermal- and Phase-Stability of All-Inorganic CSPbX<sub>3</sub> (X = Cl, Br, I) Perovskites? ACS Energy Letters. 2018;3(2):286-289.
- 47. Alam F, Wegner KD, Pouget S, Amidani L, Kvashnina K, Aldakov D, et al. Eu2+: A suitable substituent for Pb<sup>2+</sup> in CsPbX<sub>3</sub> perovskite nanocrystals? The Journal of Chemical Physics. 2019;151(23).
- 48. Yang Z, Jiang Z, Liu X, Zhou X, Zhang J, Li W. Bright Blue Light-Emitting Doped Cesium Bromide Nanocrystals: Alternatives of Lead-Free Perovskite Nanocrystals for White LEDs. Advanced Optical Materials. 2019;7(10).
- 49. Mamun AA, Ava TT, Abdel-Fattah TM, Jeong HJ, Jeong MS, Han S, et al. Effect of hot-casted NiO hole transport layer on the performance of perovskite solar cells. Solar Energy. 2019;188:609-618.
- Ali HH. Multi-Wall Carbon Nanotubes with NiO and pt as Counter Electrodes for DSSC applications. University of Thi-Qar Journal of Science. 2023;10(2):141-145.
- 51. Krupa JC, Queffelec M. UV and VUV optical excitations in wide band gap materials doped with rare earth ions: 4f–5d transitions. J Alloys Compd. 1997;250(1-2):287-292.

J Nanostruct 16(1): 375-386, Winter 2026

